Publishing House
AKAPIT

COMPUTER METHODS IN MATERIALS SCIENCE

Informatyka w Technologii Materiałów

Vol. 8, 2008, No. 3

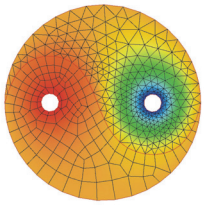

PROCESS SIMULATION OF STUB SHAFT FORGING WITH LOCAL HEATING AND COOLING – AN ANALYSIS WITH EFG

CHRISTOPH BRÖCKER*, KURT STEINHOFF, ANTON MATZENMILLER***

** Institute of Mechanics, Department of Mechanical Engineering, University of Kassel, Mönchebergstr. 7, 34125 Kassel, Germany*
*** Institute for Production Technology and Logistics, Chair of Metal Forming Technology, University of Kassel, Kurt-Wolters-Str. 3, 34125 Kassel, Germany*
Corresponding Author: amat@ifm.maschinenbau.uni-kassel.de (A. Matzenmiller)

Abstract

Within the Collaborative Research Centre SFB/TRR 30 a stub shaft is produced by applying the highly innovative metal forming technology of the simultaneous hot and cold forging in combination with a hardening process performed directly in the closed forging dies after the forging step. This complex forging process is completely simulated with the finite element code LS-DYNA including the local inductive heating phase of the workpiece as well as the rapid cooling process under pressure of the final stub shaft inside the forging dies. A new meshless element formulation denoted as element-free Galerkin method (EFG) is successfully applied to the forging process in addition to the simulation with standard finite elements. The process of the inductive heating is modelled in a simplified way. The simulation results are validated by means of experimentally measured data, showing good agreement.

Key words: simultaneous hot/cold forging, thermo-mechanically coupled FEM, meshless methods, element-free Galerkin method (EFG)

1. INTRODUCTION

Innovative and efficient production technologies must be continuously developed and advanced. For this purpose simultaneous hot/cold forging is applied in bulk metal forming and the occurring thermo-mechanically coupled phenomena are investigated within the Collaborative Research Centre Transregio 30 (SFB/TRR 30). A shaft is inductively heated only locally for forging a flange with a large diameter in the centre of the workpiece, besides the cold forging of the conical ends of the shaft (Weidig et al., 2008). Due to the inductive heating, a local austenitisation takes place in the centre of the shaft. This fact is utilised in the successive hardening process, which is performed directly within the forging dies under pressure. The possibilities and limitations of adjusting locally graded material properties in the workpiece are investigated at this forging process with differentiated cooling. The idea of this new forming strategy with simultaneous hot and cold forging has been outlined by Weidig et al. (2000) and Weidig et al. (2001). Further investigations with locally heated specimens with different heating procedures are performed e.g. by Özmen et al. (2005) and Okman et al. (2007).

For gaining a deeper understanding of the forming technology at hand and for predicting such process behaviour in advance, especially the temperature evolution in the workpiece, the entire process is investigated by means of numerical simulations. A detailed thermo-mechanically coupled finite element

ISSN 1641-8581

analysis is carried out with the commercial code LS-DYNA (Hallquist, 2007) including all process steps, i.e. heating, forging and cooling of the workpiece. Until now, the phase transformations during the cooling step can not yet be predicted by the simulation, however, if the temperature field evolution in the workpiece is known, the resulting microstructure of the material may be forecast.

When the finite element method is applied to forming processes with very large deformations, often difficulties occur due to badly distorted element meshes which can lead to inaccurate theoretical results or to an abrupt early break down of the simulation. Remeshing during the calculation can be one way to overcome these problems. However, it can be also quite difficult to create an adequate new mesh and further the remapping of the results from the old to the new mesh can lead to significant inaccuracies and artificial smoothing of the gradients of the spatial fields for the mechanical variables.

Nowadays, novel meshfree element technologies are available like the element-free Galerkin (EFG) method, which only needs discrete nodal values for the approximation of the displacement field, however, these nodes are completely independent of a finite element mesh. The EFG method was decisively developed in Belytschko et al. (1994) and Belytschko et al. (1996). An overview of element-free methods is given in Huerta et al. (2004).

By means of the EFG formulation a local adaptive refinement step is possible in principle by just introducing new nodes or eliminating old nodes, respectively, because no compatible finite element mesh is required for the nodal interpolation. The EFG method can be embedded into the standard finite element scheme, however, the handling of boundary conditions and contact is more complicated than with the FEM – see Krongauz and Belytschko (1996).

The EFG method has been recently applied to other metal forming processes – see e.g. Alfaro et al. (2006), Shangwu et al. (2005), Rossi et al. (2007), Yanjin et al. (2008). Also LS-DYNA provides an EFG element formulation (Hallquist, 2006) and it has been already used for forging analysis (Lu & Wu, 2006). The EFG method is applied also to the forging process at hand in addition to the FEM, since very large deformations occur in the centre of the flange.

In the following sections the experimental manufacturing procedure of the stub shaft is described at first. Thereupon, the constitutive model and the analysis strategy for LS-DYNA are presented shortly besides the model for the inductive heating. The next section summarises fundamental principles of the EFG method and points out its differences with respect to the FEM. Afterwards results of the FE analysis for the temperature field and the equivalent stress are visualised. Finally, the simulation results of both the FEM and EFG method are compared to each other as well as to the experimentally measured data.

2. HOT/COLD FORGING PROCESS

A cylindrical workpiece with a length of 200mm and a diameter of 30mm is made of the low alloyed steel 51CrV4 in a soft annealed state – see Weidig et al. (2008). It is heated inductively in the middle part of the shaft, see figure 1. Since the heat production concentrates in the surfaces' near zone due to the skin effect, a heat conduction phase follows with a strongly reduced heating power (35% of initial value) in order to achieve a more homogeneous temperature distribution throughout the cross-section from the boundary up to the centre of the workpiece. The maximum temperature reached during the heating process amounts to 1350°C.

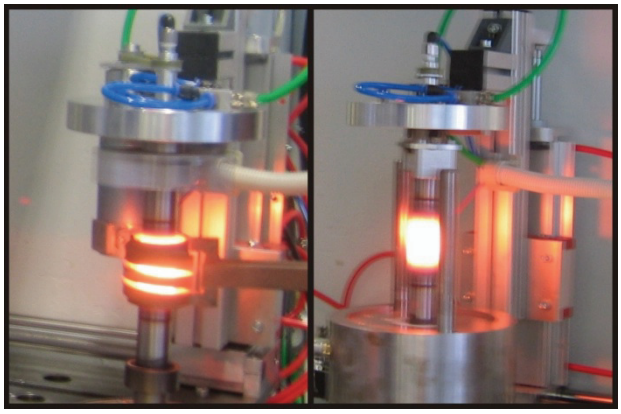

Fig. 1. *Inductive heating of shaft.*

Afterwards the workpiece is automatically transported from the induction coil into the lower forging die, followed by the downward motion of the upper die. When forging starts the maximum temperature has dropped to 1120°C. Initially, free forging of the shaft causes a uniform bulge in the heated zone, see figure 2. At the same time, the conical endings of the workpiece are formed by cold forging under the influence of a lubricant for reducing the friction. The free forming turns into tool shape determined forging with contact between the bulged material in the middle part of the shaft and the dies, where the

flange area develops. Finally, the forming process slows down when the pressing force reaches its achievable maximum of $1000kN$.

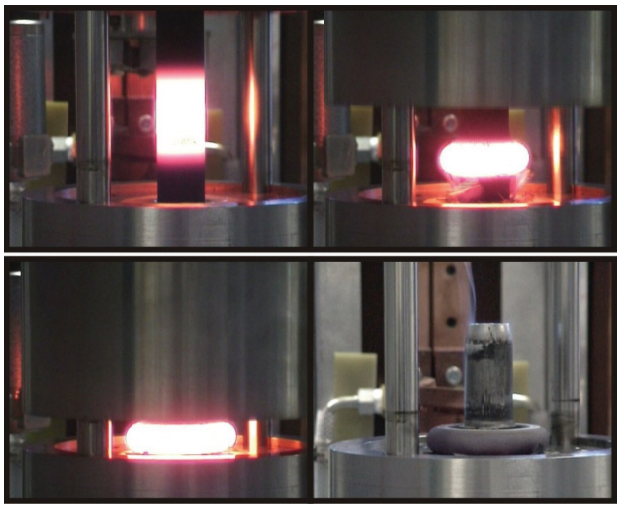

Fig. 2. *Forging of stub shaft.*

However, during the cooling process of the workpiece, the forging dies remain closed under pressure to ensure a sufficiently high heat transfer coefficient during the forced contact between the workpiece and the dies. Thus, a high cooling rate is achieved which causes an advantageous phase transformation of the austenitised material into the martensitic microstructure, where a very high strength in the flange area of up to $750HV1$ (VICKERs hardness) is measured (Weidig et al., 2008). Table 1 summarises the temporal course of the entire process.

Table 1. *Temporal course of process.*

Main heating time	12s
Heat conduction phase	5s
Transport of workpiece	6.8s
Forging	3.2s
Cooling under pressure	28s
Process time	55s

3. CONSTITUTIVE MODEL AND ANALYSIS STRATEGY

After a short introduction of the basic equations of thermoplasticity, the simulation model is discussed briefly. The coupled thermo-mechanical initial boundary value problem consists of the well-known moment balance equation with displacement and force boundary conditions and the simplified heat conduction equation on the basis of FOURIER's assumption for the heat flow vector:

$$\rho c_d \dot{T} = k\,\mathrm{div}\,(\mathrm{grad}\,T) + q^m \qquad (1)$$

with the source term:

$$q^m = \rho r + \gamma\,\sigma_{ij}\dot{\varepsilon}^p_{ij} \qquad (2)$$

and the thermal boundary conditions for free convection and radiation:

$$q_s = \varepsilon_s\,\sigma_s\,(T^4 - T_\infty^4), \quad q_L = \alpha_L\,(T - T_\infty). \qquad (3)$$

It is ρ the mass density, c_d the specific heat capacity, T the temperature and k the thermal conductivity. The heat source term q_m includes a spatial, specific heat source r, for example due to inductive heating, and the plastic stress power $\sigma_{ij}\dot{\varepsilon}^p_{ij}$ multiplied with the so-called Taylor-Quinney coefficient γ, which limits the portion of the plastic stress power, dissipated into heat. Further, σ_{ij} is the CAUCHY stress tensor, $\dot{\varepsilon}^p_{ij}$ is the plastic strain rate and in the equations for the thermal boundary conditions α_L is the convective heat transfer coefficient, T_∞ is a reference temperature, ε_S is the emissivity and σ_S the Stefan-Boltzmann constant.

The entire process is simulated completely in a single thermo-mechanically coupled analysis, comprising the three process parts: electro-magnetic heating with a simple heat source model, free and tool shape determined forging and finally rapid cooling in the closed dies.

Due to the axial symmetry of the entire process, it suffices to generate a quarter of the workpiece and the forging dies as a 3D model. In order to account for the cooling effect of the workpiece due to the heat transport into the forging dies, a thermo-mechanical contact is defined between the workpiece and the forging dies based on the penalty method. The dies are also modelled three-dimensionally but mechanically treated as rigid bodies. A simple plasticity model with isotropic hardening is chosen, where the yield stress is input by means of an experimental flow curve at a reference temperature and downscaled by the specific multiplier for every temperature level of the experimental flow curves with linear interpolation between two temperature levels. The flow curves are taken from Meyer-Nolkemper (1978). It is assumed that 95% of the plastic work are converted into heat. Thermal strains due to temperature changes are included in the constitutive model and of course, it is accounted for the thermal boundary conditions due to free convection and radiation. The simulation parameter are summarised in table 2.

Table 2. *Simulation parameters.*

YOUNG's modulus E	2.1e11 N/m^2
POISSON's ratio υ	0.3
Thermal expansion coeff. α	1.3e-5 $1/K$
Mass density ρ	7850 kg/m^3
Specific heat capacity c_d	450 $J/(kg\ K)$
Thermal conductivity (workpiece) k_W	45 $W/(m\ K)$
Thermal conductivity (dies) k_D	25 $W/(m\ K)$
Contact heat transfer coeff. h	3000 $W/(m^2K)$
Contact friction coeff. μ_C	0.08
Convective heat transfer coeff. α_L	25 $W/(m^2K)$
Emissivity ε_S	0.3
Reference temperature T_∞	300 K
Taylor-Quinney coeff. γ	0.95

The forging of the process is carried out under displacement control by prescribing the experimentally measured motion of the upper forging die for the simulation model. When reaching a total pressing force of $1000kN$, the external load agency is switched to force control like in the experiment, and the pressing force is held constant until the end of the hardening process.

An implicit time integration method is applied for calculating the displacement field during the heating and cooling phase. However, for the forging process a changeover to explicit time integration with mass scaling is performed. The temperature field is computed exclusively by implicit time integration. For the spatial discretisation in the FE simulation an 8-node element with tri-linear shape functions is employed with reduced integration and a stiffness based stabilisation method for the hourglass control – see Hallquist (2006). In the EFG formulation a Lagrangian kernel with cubic spline functions is used with a spatial full integration procedure and a treatment for essential boundary conditions based on the modified maximum entropy method – see Guo et al. (2008).

4. MODELLING OF INDUCTIVE HEATING

As already mentioned, the heat production, caused by the eddy currents during the inductive heating, takes place in a thin surface layer of the workpiece with a penetration depth ζ for the cylindrical bodies according to Brokmeier (1966), Fleck and Schönbohm (2004) or EFD Härterei (2006) of:

$$\zeta = \sqrt{\frac{\beta}{\pi f \mu_0 \mu_r}}\,, \tag{4}$$

where β is the specific electrical resistance of the workpiece which rises with the increasing temperature. f is the frequency of the electrical current in the induction coil and μ_0 is the magnetic field constant. Further, μ_r is the relative permeability of the workpiece which decreases in ferromagnetic substances, e.g. in the steel 51CrV4 used here, when the temperature increases. Finally, when exceeding the CURIE-temperature at approximately $770°C$, μ_r drops to nearly one (Gottstein, 1998). With estimations for β and μ_r according to the proposals in Richter (1983) and Hünicke and Möller (2003), the penetration depth is calculated for example at three typical temperature levels of this process – see also EFD Härterei (2006) – to:

$$\varsigma(20°C) \approx 0.075mm\,, \quad \varsigma(770°C) \approx 4.1mm\,,$$

$$\varsigma(1100°C) \approx 5.2mm\,.$$

However, for the finite element model it is assumed that the inductive heat production takes place only within a layer of $1mm$ thickness underneath the surface in the middle part of the workpiece with a height according to the length of the inductance coil of $60mm$. A volumetric heat source density ρr – see eq. (3) – is prescribed for the main heating in this surface layer with a value of $\rho r = 2600MW/m^3$ found by parameter studies and their comparison to experimental temperature measurements. During the heat conduction phase, only 35% of this value are applied according to the experimental setting.

5. ELEMENT-FREE GALERKIN METHOD (EFG)

The fundamental principles of the EFG method are shortly introduced and important differences to the FEM will be discussed.

The EFG method is based on the moving least square approximation – see Belytschko et al. (1994), Zienkiewicz and Taylor (2000), where the weight function is defined not only for one fixed point but for every location $\mathbf{x}$ of the complete interpolation domain.

An approximation function is given as:

$$u(\mathbf{x}) = \sum_{j=1}^{m} p_j(\mathbf{x}) a_j = \mathbf{p}^{\mathsf{T}}(\mathbf{x})\,\mathbf{a}\,, \tag{5}$$

with $p_j(\mathbf{x})$ as linearly independent polynomial functions and $\mathbf{a}$ as the polynomial coefficients, which

will become a function of the spatial position **x** in the following steps. With the definition of the weighted L_2-norm

$$J(\mathbf{x}) = \sum_{k=1}^{n} w_k(\mathbf{x}) \left(\mathbf{p}^{\mathsf{T}}(\mathbf{x}_k)\,\mathbf{a} - u_k\right)^2 \qquad (6)$$

the function $u(\mathbf{x}_k)$ can be fitted to the values of u_k by minimising J with respect to the unknown coefficients **a** according to:

$$\frac{\partial J}{\partial \mathbf{a}} = \sum_{k=1}^{n} w_k(\mathbf{x})\, \mathbf{p}(\mathbf{x}_k)\left(\mathbf{p}^{\mathsf{T}}(\mathbf{x}_k)\,\mathbf{a} - u_k\right) = 0\,, \qquad (7)$$

where $\mathbf{x}_k$ are the coordinates of the point with the value u_k. The weight function has the property of being equal to one at the point $\mathbf{x}_k$ and diminishes monotonically to zero with a growing distance in a defined neighbourhood about $\mathbf{x}_k$. Outside of this domain, it is zero. Such a typical weighting function is

$$w_k(r) = \begin{cases} \frac{e^{-cr^2} - e^{-cr_m^2}}{1 - e^{-cr_m^2}} & \text{for} \quad 0 \le r \le r_m\,,\ c > 0 \\ 0 & \text{for} \quad r > r_m \end{cases}, \qquad (8)$$

where $r = |\mathbf{x} - \mathbf{x}_k|$ is the radius and r_m is the support size of the weighting function, i.e. all nodes within the sphere of radius r about the point $\mathbf{x}_k$ contribute to the calculation of the value from the function $u(\mathbf{x})$ at the location $\mathbf{x}_k$. The introduction of

$$\mathbf{H}(\mathbf{x}) = \sum_{k=1}^{n} w_k(\mathbf{x})\, \mathbf{p}(\mathbf{x}_k)\mathbf{p}^{\mathsf{T}}(\mathbf{x}_k) \qquad (9)$$

and

$$\mathbf{g}(\mathbf{x}) = \sum_{k=1}^{n} w_k(\mathbf{x})\, \mathbf{p}(\mathbf{x}_k) u_k = \mathbf{h}(\mathbf{x})\mathbf{u} \qquad (10)$$

with

$$\mathbf{h}(\mathbf{x}) = [w_1(\mathbf{x})\mathbf{p}(\mathbf{x}_1)\ w_2(\mathbf{x})\mathbf{p}(\mathbf{x}_2)\ \ldots\ w_n(\mathbf{x})\mathbf{p}(\mathbf{x}_n)]\,,$$
$$\mathbf{u}^{\mathsf{T}} = [u_1\ u_2\ \ldots\ u_n] \qquad (11)$$

leads equation (8) into

$$\mathbf{H}(\mathbf{x})\,\mathbf{a} = \mathbf{g}(\mathbf{x})\,. \qquad (12)$$

Thus, the unknown polynomial coefficients **a** can be determined according to:

$$\mathbf{a} = \mathbf{H}^{-1}(\mathbf{x})\,\mathbf{g}(\mathbf{x}) \qquad (13)$$

and, h1ence, to the approximation of the function $u(\mathbf{x})$ of equation (5) results to:

$$u(\mathbf{x}) = \mathbf{p}^{\mathsf{T}}(\mathbf{x})\,\mathbf{H}^{-1}(\mathbf{x})\,\mathbf{h}(\mathbf{x})\,\mathbf{u}\,. \qquad (14)$$

The function $u(\mathbf{x})$ is an optimal approximation for the nodal values u_k with respect to the chosen norm and the weight function – on the other hand, it holds that a specified function $u(\mathbf{x})$ is best represented by the nodal values u_k and the interpolation given in equation (14). This equation can be rewritten as:

$$u(\mathbf{x}) = \mathbf{N}(\mathbf{x})\mathbf{u}\,, \qquad (15)$$

where

$$\mathbf{N}(\mathbf{x}) = \mathbf{p}^{\mathsf{T}}(\mathbf{x})\,\mathbf{H}^{-1}(\mathbf{x})\,\mathbf{h}(\mathbf{x}) \qquad (16)$$

are the EFG shape functions obtained from the moving least square method. Thus, compared to the FEM a formally similar form for the approximation of the displacement functions is obtained. The EFG method approximates the displacement field analogous as in the FE-method for discretising the weak formulation of the momentum balance equations. Note, the EFG method as well as the FEM satisfy the partition of unity, i.e.

$$\sum_{j=1}^{m} N_j(\mathbf{x}) = 1\,. \qquad (17)$$

This is an important property for the numerical integration of the EFG weak formulation, which is performed slightly differently compared to the FEM – see Beissel and Belytschko (1996). Further, considerable differences exist with the EFG method in contrast to the FEM. There is much more computational effort needed for the calculation of the EFG shape functions, which are defined not only locally for every single element, as in the case of the FEM, but have a value between zero and one at several nodal positions in the vicinity of the test point $\mathbf{x}_k$. The FEM enforces $N_i(\mathbf{x}_j) = \delta_{ij}$, which leads to $u(\mathbf{x}_i) = u_i$. This enables an easy way of prescribing the essential boundary conditions. However, for the EFG it is $N_i(\mathbf{x}_j) \neq \delta_{ij}$, and, thus, in general: $u(\mathbf{x}_i) \neq u_i$. Further, the sum of all shape functions is less than one at the boundaries. Hence, Lagrange multipliers or special, new methods must be applied to enforce the essential boundary conditions, see Krongauz and Belytschko (1996).

LS-DYNA provides different options for e.g. the boundary treatment or the definition of the kernel functions – see Hallquist (2007). For instance, even an Eulerian formulation – see Ponthot and Belytschko (1998) – for the EFG kernel function is available.

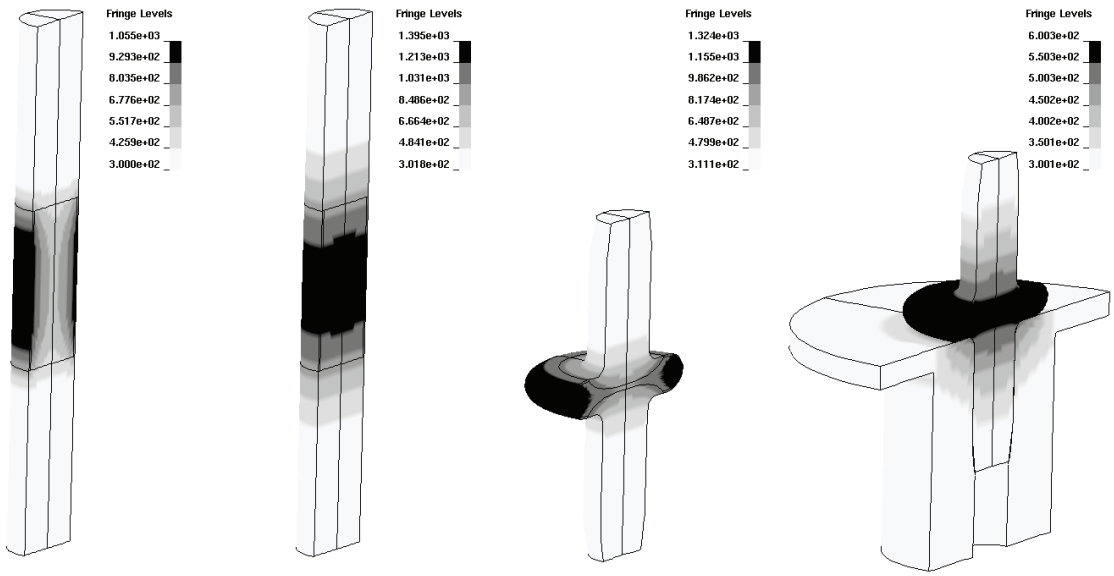

Fig. 3. *Temperature field (in Kelvin) during heating (picture 1), at beginning of forging (picture 2), at end of forging (picture 3), at end of cooling process (picture 4).*

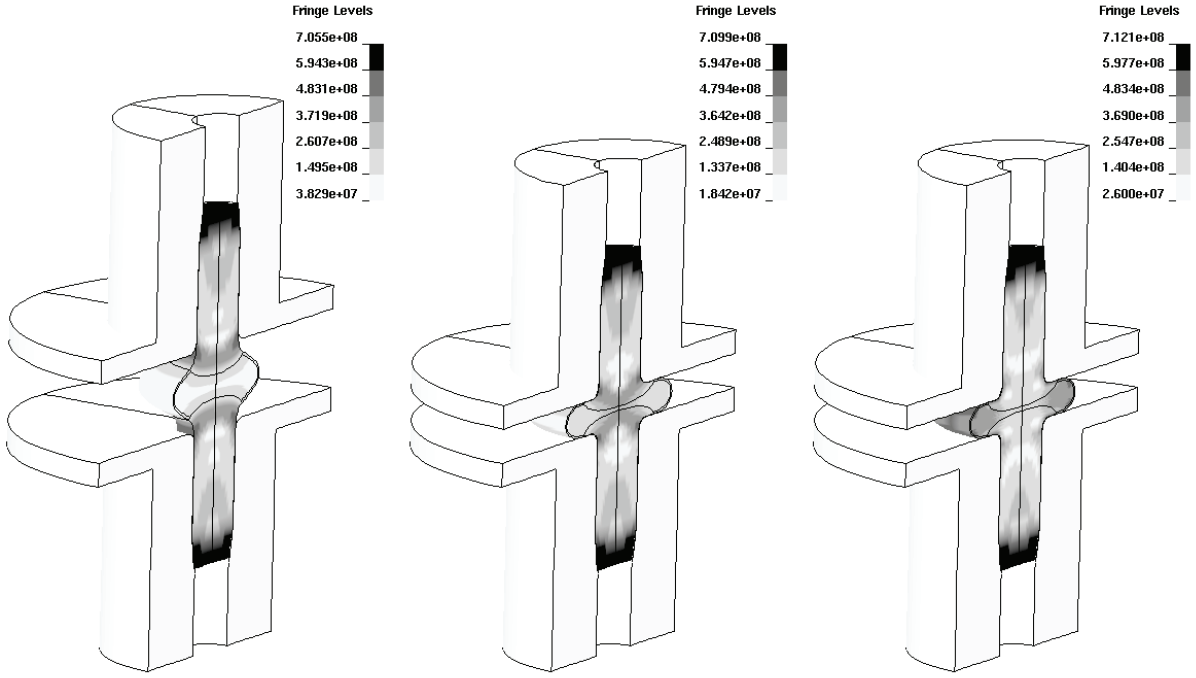

Fig. 4. *Equivalent stress according to von Mises during forging (picture 1), at end of forging (picture 2), at end of cooling process (picture 3).*

6. RESULTS OF FEM

The temperature field, calculated in the FE-simulation, is shown for the workpiece in figure 3. The first picture presents the temperature distribution at the beginning of the heating process. The surfaces' near zone is already heated up strongly, whereas the interior of the shaft is still much colder. When forging starts (picture 2), a fairly homogeneous temperature field with a maximum of approximately 1100°*C* is found over the cross-section. However, a strong temperature gradient may be stated in the axial direction. According to the high temperatures in the centre of the shaft, the initial yield stress is strongly reduced there. The hot material is squeezed outwards during forging and forms the flange. Thus, at the end of forming (picture 3), the temperature in the centre is quite lower than in

the outer flange region. Due to the contact of the hot workpiece with the cold dies, the heat is transported massively out of the workpiece into the forging dies which causes a high cooling rate in the workpiece. Picture 4 shows the temperature distribution in the workpiece and in the forging die at the end of the simulation at $t = 55s$, where only the lower forging die is sketched for the reason of clarity.

Figure 4 presents the distribution of equivalent stresses in the workpiece during forging and at the end of the cooling process. Picture 1 and 2 show that the highest stresses evolve when the conical endings of the shaft are formed by cold forging at a high hydrostatic pressure. Despite large straining during the deformation of the flange, the stress level is relatively low due to the high temperatures in the forging zone. However, the eigen stresses in the flange area augment during the forced cooling of the workpiece (picture 3).

7. FORGING SIMULATION WITH EFG

The EFG element formulation is applied to the process simulation at hand for the calculation of the displacement field. Adaptivity of the nodal values is not yet accounted for in this early EFG study, and postponed to future work. The computational costs are much higher, but accurate results are ensured in the simulation with the EFG method, whereas in the FE analysis locally large deformations with distorted elements occur in the centre of the flange. However, the simulation results of both methods are quite close and agree well with the measured data from the experiment.

Figure 5 and 6 show the temperature and equivalent stress distribution at the end of the forging process in the EFG simulation, where the nodal values are illustrated as coloured spheres.

Figure 7 shows the comparison of the pressing force and the displacement of the upper die, measured in the experiment and calculated from the simulation with both the FE and EFG method. At a point in time of approximately 20s, the upper die of the forging press starts to move down in the experiment. However, a significant nonzero pressing force is already recorded by the measuring devices, although there is no contact to the workpiece yet, since the upper forging die reaches the workpiece first at time $t = 23.8s$. The subsequently evolving force in the test agrees reasonably well with the pressing load, calculated in the simulations.

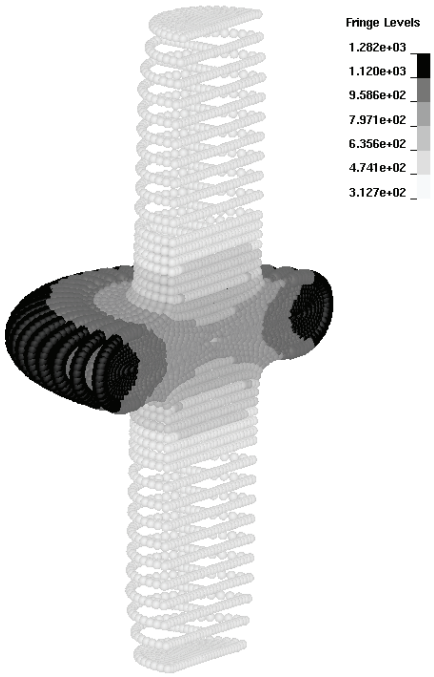

Fig. 5. *Results of EFG simulation: nodal values of temperature at end of forging.*

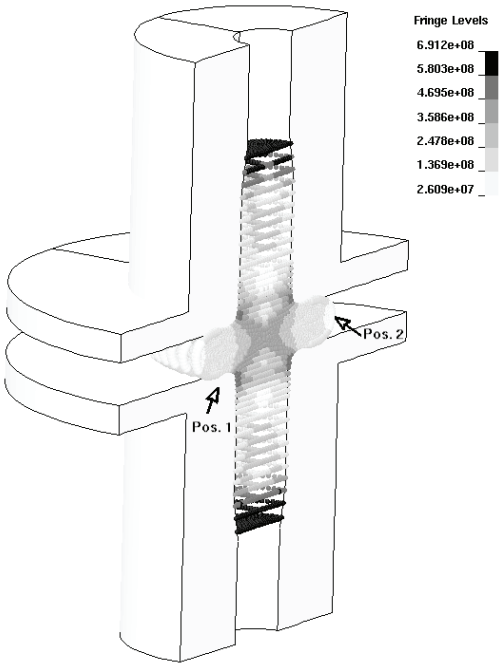

Fig. 6. *Results of EFG simulation: nodal values of equivalent stress according to von Mises at end of forging. Temperature measuring positions of experiment are marked.*

During the forging and cooling process, the temperature is recorded by means of thermocouples in the forging die (see figure 6, position 1) as well as contactlessly on the flange surface of the shaft with a spatial fixed pyrometer (figure 6, position 2). The results of the temperature measurement are presented in figure 8 and compared to the simulation results. Since the pyrometer is fixed just above the lower die (see figure 6, position 2), the recorded

temperature can be interpreted initially at that time when the flange forming is nearly finished. The lower limit for the measurement range of the pyrometer is at least 400°C, thus, no further temperature drop can be reported after it passes this limit. Over all, the calculated temperatures at the flange are in excellent accordance with the pyrometer temperature data. The experimental recorded temperature in the die agrees qualitatively well with the simulated temperature evolution in time. However, the temperature values, determined in the simulation, are lower then the ones received from the experiment.

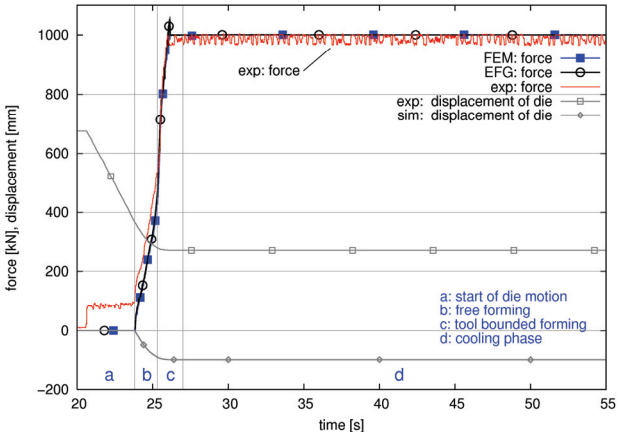

Fig. 7. *Comparison of forming force for FEM, EFG and experiment; additionally displacement of upper die is plotted.*

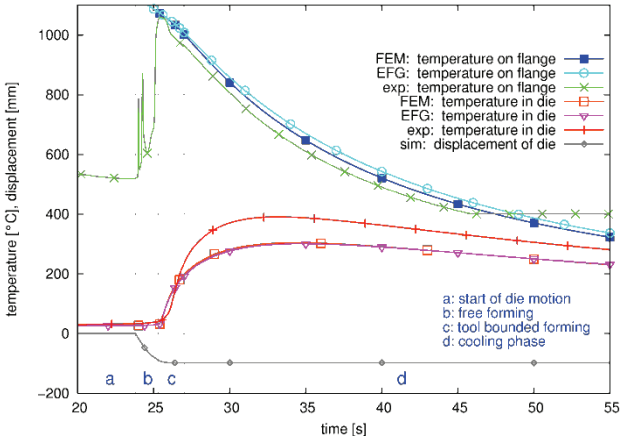

Fig. 8. *Comparison of temperature on flange and in die for FEM, EFG and experiment; additionally displacement of upper die is plotted.*

Table 3 presents the geometrical data, sketched in figure 9 of the final stub shaft and its percental deviation, which also states that the results between the FEM and the EFG method are quite close and that the agreement between simulation and experiment is satisfactory.

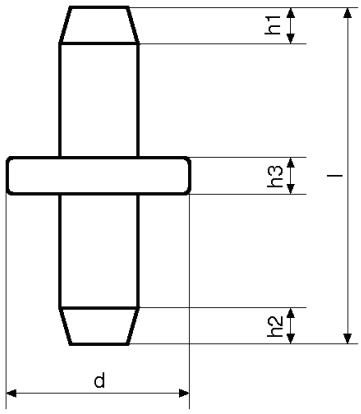

Fig. 9. *Sketch of final stub shaft.*

Table 3. *Comparison of geometrical data.*

	Experiment [mm]	Simulation [mm]		Disagreement [%]	
		FEM	EFG	FEM	EFG
h1	12.0	13.8	11.9	15.0	-0.8
h2	14.0	13.7	11.8	-2.1	-15.7
h3	13.6	14.2	14.3	4.4	5.1
d	76.8	77.5	78.4	0.9	2.1
l	130.6	131.7	127.9	0.8	-2.1

8. SUMMARY AND CONCLUSIONS

The simultaneous hot/cold forging is applied to the production of a stub shaft with a subsequent hardening process in the forging press. This complete forming procedure is numerically analysed with the finite element code LS-DYNA including the heating, forging and cooling step. Besides the FE-analysis, another novel meshless element approach, denoted as element-free Galerkin (EFG) method, is used, whose theoretical background is explained briefly. The simulation results are presented and both FE and EFG methods are compared to each other, showing similar results. Further, a good or even excellent agreement can be observed in the final comparison to the experimental data.

The FEM is generally applicable and efficient for metal forming analyses. However, difficulties appear when very large deformations occur and elements become badly distorted during the simulation of the process, which makes remeshing necessary. The EFG method is always more accurate at a higher numerical cost compared to the FEM, since no compatible mesh with a regular element geometry is required for this method and, moreover, higher order polynomials may be used for the kernel functions. Thus, stiffening due to badly distorted elements is circumvented and there is no need for remeshing due to the loss of accuracy in distorted elements. Fur-

thermore, local adaptivity is possible by just introducing new nodes or eliminating old ones, which is, however, not yet applied in this study.

For this special process of simultaneous hot/cold forging it is shown that the global results of both methods agree quite well with each other, which confirms the results and the applicability of the finite element simulation in this case. However, besides the much larger computation time with EFG, there is in fact a difference in the centre of the workpiece, where the elements in the FE simulation suffer under a very small thickness to length aspect ratio. The EFG simulation shows in close agreement with the experiment the excessive compression of the initially heated part of the shaft, whereas the finite element result underestimates the strong longitudinal distortion. That means, the finite element response stiffens in this area due to the poor element geometry. However, this difference between the EFG and FEM results has only a local influence on the flow process and does nearly not effect the global forming result, like the final geometry of the flange or the total force in the press.

ACKNOWLEDGEMENT

This publication is based on research activities of the collaborative research centre SFB/TR TRR 30 “Process integrated production of functionally graded structures on the basis of coupled thermo-mechanical phenomena”, which is kindly supported by the German Research Foundation (DFG).

REFERENCES

Alfaro, I., González, D., Bel, D., Cueto, E., Doblaré, M., Chinesta, F., 2006, Recent advances in the meshless simulation of aluminium extrusion and other related forming processes, *Arch. Comput. Meth. Eng.*, 13 (1), 3-43.

Beissel, S., Belytschko, T., 1996, Nodal integration of the element-free Galerkin method, *Comput. Meth. Appl. Mech. Eng.*, 139, 49-74.

Belytschko, T., Krongauz, Y., Organ, D., Fleming, M., Krysl, P., 1996, Meshless methods: An overview and recent developments, *Comput. Meth. Appl. Mech. Eng.*, 139, 3-47.

Belytschko, T., Lu, Y.Y., Gu, L., 1994, Element-free Galerkin methods, *Int. J. Numer. Meth. Eng.*, 37, 229-256.

Brokmeier, K.-H., 1966, *Induktives Schmelzen*, W. Girardet, Essen (in German).

EFD Härterei F. Düsseldorf GmbH, 2006, *Grundlagen der Induktionshärtetechnik, Härtereihandbuch*, date of version: 07.04.2006, www.efd-haerterei.de/pdf/HH-R01-D06-Induktionstechnik.pdf (in German).

Fleck, C., Schönbohm, A., 2004, Entwurf einer flachheitsbasierten Vorsteuerung für die induktive Erwärmung beim Thixoforming, *Automatisierungstechnik*, 52 (9), 403-410 (in German).

Gottstein, G., 1998, *Physikalische Grundlagen der Materialkunde*, Springer, Berlin (in German).

Guo, Y., Wu, C.T., Xu, J., Lu, H., 2008, Element Free Galerkin EFG – Meshless Methods in LS-DYNA: Current, Future and Industrial Applications, *ANSYS Conference & 26th CADFEM Users' Meeting*, eds, CADFEM GmbH, October 22 - 24, 2008, Darmstadt/Germany.

Hallquist, J.O., 2006, *LS-DYNA Theory Manuel*, Livermore Software Technology Corporation.

Hallquist, J.O., 2007, *LS-DYNA Keyword User's Manuel*, Livermore Software Technology Corporation.

Huerta, A., Belytschko, T., Fernández-Méndez, S., Rabczuk, T., 2004, Meshfree Methods, *Encyclopedia of Computational Mechanics*, eds, Stein, E., de Borst, R., Hughes, T.J.R., John Wiley & Sons, Ltd, 1-49.

Hünicke, U.-D., Möller, S., 2003, Auswertung der statischen Magnetisierungskurve zur Kontrolle von Gefüge- und Behandlungszuständen bei Stählen, *Proceedings of DGZfP-Annual Conference Meeting*, eds, DGZfP, Mainz (in German).

Krongauz, Y., Belytschko, T., 1996, Enforcement of essential boundary conditions in meshless approximations using finite elements, *Comput. Meth. Appl. Mech. Eng.*, 131, 133-145.

Lu, H.S., Wu, C.T., 2006, A Grid-based Adaptive Scheme for the Three-Dimensional Forging and Extrusion Problems with the EFG Method, *9th Int. LS-DYNA Users Conference*, eds, LSTC, Dearborn, Michigan, USA, 17/33-17/44.

Meyer-Nolkemper, H., 1978, *Fließkurven metallischer Werkstoffe*, HFF-Report No. 4, Hannoversches Forschungsinstitut für Fertigungsfragen e. V., (in German).

Okman, O., Özmen, M., Huwiler, H., Tekkaya, A. E., 2007, Free forming of locally heated specimens, *Int. J. Mach. Tool. Manufact.*, 47, 1197-2005.

Özmen, M., Okman, O., Huwiler, H., Tekkaya, A. E., 2005, Forming of Complicated Shapes by Local Heating, *8th ICTP*, eds, Bariani, P. F., October 9-13, 2005, Verona/Italy, 1-8.

Ponthot, J.-P., Belytschko, T., 1998, Arbitrary Lagrangian-Eulerian formulation for element-free Galerkin method, *Comput. Meth. Appl. Mech. Eng.*, 152, 19-46.

Richter, F., 1983, *Physikalische Eigenschaften von Stählen und ihre Temperaturabhängigkeit*, Stahleisen-Sonderbericht, Heft 10, Publisher Stahleisen m. b. H., Düsseldorf, (in German).

Rossi, R., Alves, M.K., Al-Qureshi, H.A., 2007, A model for the simulation of powder compaction processes, *J. Mater. Process. Tech.*, 182, 286–296.

Shangwu, X., Rodrigues, J.M.C., Martins, P.A.F., 2005, Simulation of plane strain rolling through a combined element free Galerkin-boundary element approach, *J. Mater. Process. Tech.*, 159, 214-223.

Weidig, U., Kayatürk, K., Kurt, A., Steinhoff, K., Tekkaya, A. E., 2000, Combination of Cold and Hot Forging in a Single Forming Step: Production Technique, Workpiece Geometries, Material Characteristics, *Proceedings of the 14th International Forgemasters Meeting*, Wiesbaden/Germany, September 3-8, Publisher Stahleisen m. b. H., Düsseldorf, 199-206.

Weidig, U., Steinhoff, K., Tekkaya, A. E., 2001, Simultaneous cold and hot forging in a single step, *Wire*, 51 (2), 58-60.

Weidig, U., Hübner, K., Steinhoff, K., 2008, Bulk steel products with functionally graded properties produced by differential thermo-mechanical processing, *Steel Res. Int.*, 79 (1), 59-65.

Yanjin, G., Xin, W., Zhao, G., Ping, L., 2008, A nonlinear numerical analysis for metal-forming process using the rigid-(visco)plastic element-free Galerkin method, *Int. J. Adv. Manuf. Tech.*, DOI 10.1007/s00170-008-1585-3, available from: http://www.springerlink.com/content/c6453224m4270411/ (last accessed: 15.12.2008).

Zienkiewicz, O.C., Taylor, R.L., 2000, *The Finite Element Method, Volume 1: The Basis*, Fifth edition, Butterworth-Heinemann, Oxford.

PORÓWNANIE MODELI ZNISZCZENIA DLA PRZEWIDYWANIA PLASTYCZNEGO PĘKANIA W PROCESACH KUCIA

Streszczenie

Możliwość przewidywania plastycznego pękania odgrywa ważną rolę w projektowaniu wyrobów kutych. Badania doświadczalne pokazują, że zarodkowanie, wzrost i łączenie się pustek są mechanizmami kontrolującymi powstawanie i rozprzestrzenianie się pęknięć. Na te mechanizmy oddziałują, w różnym stopniu, takie parametry jak ciśnienie hydrostatyczne, intensywność naprężenia i maksymalne naprężenie główne. Znanych i używanych w praktyce jest wiele kryteriów pękania plastycznego opartych na tych parametrach. W niniejszej pracy te kryteria są porównywane. Spośród najbardziej popularnych wybrano kryteria pękania przynależne do różnych grup, klasyfikowane według podstaw danego kryterium, a więc kryteria oparte na mikrostrukturze materiału, kształcie pustek lub mechanizmie ich wzrostu. Kryteria oparte na mechanizmie kontinuum pękania, w których bierze się pod uwagę sprzężenie między odkształceniem plastycznym i degradacją materiału poprzez analizę różnych możliwości rozwoju zniszczenia dla rozciągającego i ściskającego stanu naprężenia, dają bardziej poprawną lokalizację obszarów, w których następuje inicjacja pęknięcia.

Received: October 8, 2007
Received in a revised form: November 6, 2007
Accepted: November 6, 2007